



Lithospheric density models reveal evidence for Cenozoic uplift of the Colorado Plateau and Great Plains by lower-crustal hydration

Will Levandowski^{1,2,3}, Craig H. Jones^{2,3}, Lesley A. Butcher^{2,3}, and Kevin H. Mahan^{2,3}

¹Department of Geology, Colorado College, Colorado Springs, Colorado 80903, USA

²Department of Geological Sciences, University of Colorado, Boulder, Colorado 80309, USA

³Cooperative Institute for Research in Environmental Sciences (CIRES), University of Colorado, Boulder, Colorado 80309, USA

ABSTRACT

Subduction at plate boundaries can have thermal, chemical, and physical impacts on broad regions of the continental interior, but these interactions are not as readily obvious as deformation near the continental margin. Such cryptic alteration has produced surface uplift in the Colorado Plateau and western Great Plains of North America, which have risen—largely undeformed—1.6 and 1.3 km, respectively, relative to the eastern Great Plains during the Cenozoic. Accumulation of Cretaceous–Cenozoic sediments accounts for only 300 m of uplift of the Colorado Plateau and 400 m of the western Great Plains, leaving 1.3 km and 0.9 km, respectively, unexplained. To determine the physical causes of this enigmatic epeirogeny, we derived three-dimensional (3-D) lithospheric density models from seismic velocity, gravity, topography, and heat-flow data. Lower-crustal density decreases systematically westward across the Great Plains, accounting nearly perfectly for the remaining 900 m of uplift of the western Great Plains and the modern east-west topographic gradient. Lower-crustal dedensification beneath the Colorado Plateau accounts for a similar 900 m of uplift. Lower-crustal xenoliths in both regions show progressive hydration-induced retrogression of garnet-bearing assemblages with increasing modern elevation, and Th-Pb dating of the Colorado Plateau retrogression gives end-Cretaceous dates (xenoliths from the Great Plains have not yet been dated). We hypothesize that lower-crustal density variations—and much of the surface relief—in North America’s Proterozoic interior terranes reflect varying degrees of metasomatic retrogression, such as by fluids exsolved from the Farallon slab. The remaining 400 m of Colorado Plateau uplift is most plausibly due to elevated mantle temperature. We present thermal models that suggest that 25–70 km of Cenozoic lithospheric thinning can explain the modern elevation and density structure.

INTRODUCTION

Paleozoic and Mesozoic marine sediments blanket the Colorado Plateau and Great Plains, requiring broadly uniform elevations near sea level through

much of the Phanerozoic. Since the Late Cretaceous, however, these units have risen—generally undeformed—to average elevations of 1.9 km in the Colorado Plateau and 1.6 km in the western Great Plains (Fig. 1A). By contrast, on the eastern Great Plains, they remain only 300 m above modern sea level. Modern topographic relief therefore reflects differential uplift, so understanding what supports this relief will provide a window into the processes responsible for the widespread but cryptic Cenozoic modification of intraplate North America.

Although the Sevier and Laramide orogenies caused substantial horizontal contraction in the modern Basin and Range and Southern Rockies, respectively, the Colorado Plateau and Great Plains experienced <5% shortening (Davis, 1978; Tikoff and Maxson, 2001). Instead, the major impact of Farallon subduction was a period of subsidence and shallow marine sedimentation (Sloss, 1963). Sediments increased crustal buoyancy beyond presubsidence values, and Tertiary removal of the Farallon slab allowed the crust to rebound to correspondingly higher surface elevation (Mitrovica et al., 1989). Digitizing the isopach maps of Cook and Bally (1975), we find that an average of 900 m of post-Jurassic sedimentary rock is preserved on the Colorado Plateau, and across the Great Plains, their average thickness grades from 1.3 km near the Rocky Mountain front to minor net erosion in eastern Kansas, Oklahoma, and Nebraska.

The isostatic contribution to topography, H , of a layer with density ρ and thickness z , compensated by asthenosphere of density ρ_a , is

$$H = z \frac{\rho - \rho_a}{\rho_a} \quad (1)$$

Assuming a density of 2000–2200 kg/m³ for these sedimentary rocks (e.g., Spencer, 1996) and asthenospheric density of 3200 kg/m³ (e.g., Lachenbruch and Morgan, 1990), they account for ~300–350 m of uplift of the Colorado Plateau relative to the eastern Great Plains and 400–500 m in the western Great Plains (Fig. 1B). In the Colorado Plateau, 1.3 km of Cenozoic uplift remain unexplained, and on the Great Plains, there is a roughly linear gradient in remaining uplift from 900 m near the Rocky Mountain front to 0 m on the eastern Great Plains.

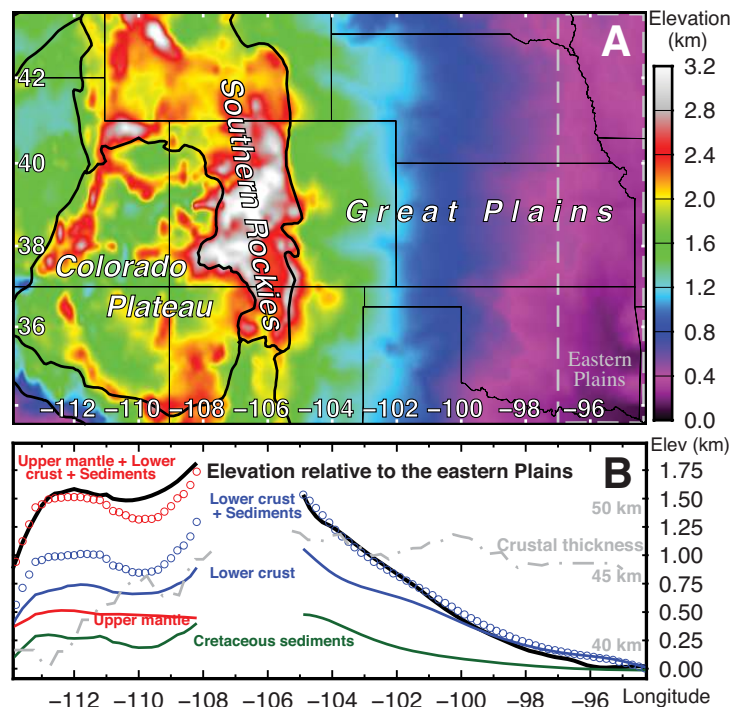


Figure 1. (A) Modern elevation of the Colorado Plateau and Great Plains. The reference region—the low-elevation eastern Great Plains—is the area east of 97°W, outlined in gray. (B) Longitudinal averages from 33.5°N to 44.5°N of surface elevation (black) and the flexurally modulated topography supported by post-Jurassic sediments (green) and modeled lower-crustal density (blue), each relative to the eastern Great Plains. These two buoyancy sources account for the modern topographic relief and thus Cenozoic differential uplift across the Great Plains. In the Colorado Plateau (curves west of 108°W, including only points in the region outlined in A), the upper mantle supports 400 m of additional relief (red). Average crustal thickness (Shen et al., 2013) is shown for reference in gray, with vertical exaggeration tantamount to an $\sim 400 \text{ kg/m}^3$ density difference between crust and mantle. Note the lack of any correlation between crustal thickness and surface elevation. The blank region from 108°W to 105°W is the Southern Rockies, which are not the subject of this paper.

Because the Colorado Plateau and Great Plains share similar Mesozoic histories and even overlie the same Proterozoic terranes (Whitmeyer and Karlstrom, 2007), systematic differences in modern density that support modern topographic relief most logically result from Cenozoic modification/deformation. The EarthScope Transportable Array (TA) has recently offered unprecedented seismic coverage of the central United States; here, we used TA-based seismic velocity models (Shen et al., 2013) along with heat-flow, gravity, and topographic data to develop three-dimensional (3-D) lithospheric density models. These estimates map and quantify the contributors to modern eleva-

tion differences—and by inference Cenozoic surface uplift—across the Great Plains and Colorado Plateau.

HYPOTHESIZED CAUSES OF UPLIFT

Surface uplift may occur in response to changes in asthenospheric flow (i.e., dynamic topography) or in response to decreases in the density of the lithosphere, which depends on both temperature and composition. Therefore, the possible causes of uplift relative to the Paleozoic–Mesozoic can be enumerated (following McGetchin et al., 1980; Morgan and Swanberg, 1985): crustal thickening, crustal heating, crustal phase changes, advective or conductive heating of the mantle, chemical or phase changes in the mantle lithosphere, or dynamic topography (here defined as a non-isostatic contribution from mantle flow, not simply mantle buoyancy).

Indeed, most of these mechanisms have been proposed for the Colorado Plateau and/or Great Plains. Nevertheless, crustal thickening (Bird, 1984; McQuarrie and Chase, 2000) seems unlikely because of the minimal shortening observed at the surface (Davis, 1978; Tikoff and Maxson, 2001). Moreover, crustal thickness (gray line in Fig. 1B) does not vary systematically across the Great Plains and is not correlated with surface elevation ($r^2 = 0.19$). While crustal heating decreases density and increases elevation, modern heat flow is a relatively uniform 50–60 mW/m^2 across the Great Plains (e.g., Blackwell and Richards, 2004). Lower-crustal and upper-mantle seismicity in the Colorado Plateau interior (Wong and Humphrey, 1989) also suggests low thermal gradients, and joint analysis of heat-flow data and P_n velocities estimates a Moho temperature of $<700 \text{ }^\circ\text{C}$ (Schutt et al., 2018). Around the margins of the Colorado Plateau, heat flow is modestly higher, up to $\sim 75 \text{ mW/m}^2$ (e.g., Blackwell and Richards, 2004), and Moho temperatures average $900 \text{ }^\circ\text{C}$ (Schutt et al., 2018), meaning that the average temperature of the Colorado Plateau Moho is $\sim 800 \text{ }^\circ\text{C}$. By contrast, temperatures of $\sim 550 \text{ }^\circ\text{C}$ typify the Great Plains (Schutt et al., 2018). Assuming a roughly linear geotherm from the Moho to the surface, our crude calculation suggests an average difference of $125 \text{ }^\circ\text{C}$. For a coefficient of thermal expansion of $3.0 \times 10^{-5}/^\circ\text{C}$ and a reference density of 2800 kg/m^3 , this difference accounts for a 10.5 kg/m^3 density difference. By Equation 1, the 40-km-thick crust of the Colorado Plateau thus supports only 130 m of additional elevation.

Each of the remaining hypotheses—dynamic topography, mantle or crustal composition/phase changes, and mantle heating—makes testable predictions about modern lithospheric seismic velocity and/or density structure, but these predictions have yet to be investigated systematically.

DENSITY MODELING

To discriminate among these remaining possibilities, we derived 3-D density models of the crust and upper mantle following the approach of

Levandowski et al. (2015), which jointly analyzed shear-wave velocity (Shen et al., 2013), gravity (Fig. 2B), topography (Fig. 1A), and heat flow. Velocity is scaled to density to create a 3-D starting density model (Fig. 3). Gravity and flexurally smoothed topography are then forward modeled (Figs. 2C–2D) and compared to observations. Finally, a random-walk Monte Carlo algorithm iteratively refines the density model until free-air gravity and flexurally smoothed topography are reproduced at all points in the study area to within 10 mGal and 100 m, respectively (Figs. 2G–2H). (L1/L2 [L1 is the mean absolute value; L2 is the root mean squared] norms are generally ~2.5/4 mGal and 30/50 m.)

Shen et al. (2013) provided hundreds of velocity models at each of ~1000 TA stations. These models comprise one-dimensional (1-D) velocity profiles and include a sedimentary thickness and crustal thickness, both of which also vary among the individual 1-D models at any given station. They were derived by joint Bayesian inversion of short-period Rayleigh wave dispersion from ambient noise, long-period dispersion from ballistic Rayleigh waves (a total range of ~8–80 s), and receiver functions. Nevertheless, there is not a unique velocity model that is capable of reproducing these data (which themselves are subject to uncertainty). In an effort to minimize the bias imposed on our density models of the vagaries of a given S-velocity model, we created 1000 simulations of the 3-D density structure, and each simulation began by randomly selecting one of the acceptable Vs models at each station and scaling these to density.

velocity-temperature-density scaling that accounts for anelasticity (using scripts provided by U. Faul; Jackson and Faul, 2010) and the presence of melt (Levandowski and Jones, 2015; Levandowski et al., 2015) for a uniform, peridotitic composition:

$$\Delta\rho = \Delta v_s \times \left(7.3 - \frac{z}{100km} + \frac{\Delta v_s}{4} \right); \Delta v_s \leq 6\%, \quad (3a)$$

$$\Delta\rho = \Delta v_s \times \left(8.8 - \frac{z}{100km} - \frac{7(\Delta v_s - 6)}{40} \right); \Delta v_s \geq 6\%. \quad (3b)$$

Here, z is depth below the surface in km, and Δv_s is the perturbation (in %) relative to some reference, v_0 , which we assume to be 4.5 km/s. Therefore,

$$\Delta v_s = 100 * \frac{v_s - v_0}{v_0}. \quad (3c)$$

Since this reference is meant to be quite near the solidus (i.e., assuming that the adiabatic temperature in the asthenosphere is quite near the solidus), velocities below v_0 may reflect increasing melt content, which does not significantly affect density. Therefore, there is a final implicit segment of the velocity-density relationship:

$$\Delta\rho = 0; \Delta v_s \leq 0\%. \quad (3d)$$

We explored the effect of different choices of v_0 in the Supplemental Material¹, but this choice can be viewed as a hypothesis to be tested. If, for example, the predicted densities of regions such as the Basin and Range or Snake River Plain with lower velocities in the mantle are too high—as manifest in topography and/or gravity—we would conclude that a lower v_0 would be indicated.

Equation 3 was derived for a composition of 30% Fo₉₀, 30% Fo₉₂, 25% orthopyroxene (opx), 10% clinopyroxene (cpx), 2.5% garnet (Gt), 2.5% spinel (Sp), and 1 mm grains, where Fo indicates the proportion of forsterite in olivine. Because the anelasticity data (Jackson and Faul, 2010) are for single-crystal olivine only, we assumed that anelastic effects were similar for other minerals. The effects of grain size and solidus velocity are addressed in the Supplemental Material (see footnote 1), but we found that our results were robust with respect to changes in these two factors. For each mineral, we accounted for the pressure and temperature dependence of the shear and bulk moduli (Bouhfid et al., 1996; Hugh-Jones, 1997; Jackson et al., 2003; Afonso et al., 2005) and for the temperature dependence of thermal expansivity (Afonso et al., 2005). To account for anelasticity, we also accounted for the temperature, pressure, and seismic period dependence of the dynamic compliance, or the Laplace transform of the creep function (using scripts provided by Jackson and Faul, 2010). Finally, the representative period of surface waves increases with depth (from ~30 s at 50 km to 80 s—the longest period used by Shen et al. [2013]—at 150 km), so these velocity-density relationships are depth dependent, both because of increasing pressure and increasing seismic period. In other words,

Initial Density Model

The velocity models of Shen et al. (2013) explicitly included a crust-mantle boundary. Therefore, it is easy to separate the crust from the mantle and use different velocity-density relationships in each. In the crust, the initial velocity-density scaling uses temperature-at-depth estimates (Blackwell et al., 2011) to separate the minor influence of thermal variations on velocity and accounts for the attendant density variations (Levandowski et al., 2013, 2015). The isothermal (i.e., composition-dependent) velocity estimate is then scaled to density using a regression based on empirical data (Christensen, 1996; Brocher, 2005):

$$\rho = -15.84v_s^5 + 209.13v_s^4 + -961.94v_s^3 + 1863.36v_s^2 + -1163.00v_s + 2153.06. \quad (2)$$

This polynomial regression—or any reasonable regression—cannot faithfully reproduce the density of all lithologies because of the natural spread in density of rocks that have similar velocity; the range in density about a given seismic velocity is approximately ±150 kg/m³. In particular, this regression systematically underestimates the density of mafic rocks and overestimates the density of felsic units (Levandowski et al., 2015).

In the mantle, the initial scaling assumes that all velocity variations are thermal in origin, and we subsequently relax this assumption. We use a

UNCERTAINTY IN DENSITY MODELS

A more complete discussion of uncertainties in density models derived similarly to ours, and the sources thereof, is given by Levandowski et al. (2017). Here, we present a brief discussion of the variability of densities in our accepted 3-D models and then turn our attention to systematic biases that may have been introduced by our assumptions and modeling procedure.

Uncertainty is readily quantified from our modeling: we have 1000 estimated densities at each point on a 20x20 km grid and in 15 different layers. Considerable care should be taken in deciding what a meaningful measure of uncertainty is, however. The density in any one 5x20x20 km cell in the lower crust of our model is not important. The meaningful quantity is the density across multiple layers in our model, say the 20–40 km range. Also, because our primary goal is to investigate the long-wavelength topographic gradient that has developed on the Plains in the Cenozoic, we are chiefly interested in average densities along a line of longitude. As such, we should consider that an individual 100-km wide swath of lower crust subsamples a grid ~55 nodes from north to south, 5 nodes from east to west, and 4 layers thick. If the densities of these ~1100 cells are independent of one another (not a terrible approximation, as determined from statistical tests that are not shown here), then the uncertainty of that volume is roughly 1/33 the uncertainty of any given cell. Considering the differences in modeled density across the Plains (>100 kg/m³), one would require that the uncertainty in a typical cell be 3300 kg/m³, which is non-physically large: it would require the assertion that our modeling cannot tell whether there is air or arhenosphere at any given point.

We now discuss the uncertainty in the density over a given depth range at any of our 20x20 km columns. Beyond the upper few km, uncertainty is highest near the Moho, so we will discuss results from this depth range. The density in, say, the 40–50 km depth range varies in any given column across the 1000 simulations, mainly controlled by how uncertain the Moho depth is. For a typical point, 950 of the 1000 density models are within 30–40 kg/m³ of the mean value from across all of the 1000 models. If we consider the depth range from 30–50 km, uncertainty is typically ±25 kg/m³. The 20–50 km depth range primarily discussed in the text typically has uncertainties of 15–20 kg/m³. Again, these values are the 95%

¹Supplemental Material. Additional discussion of the potential influences of systematic biases in the density modeling. Please visit <http://doi.org/10.1130/GES01619.S1> or the full-text article on www.gsa-pubs.org to view the Supplemental Material.

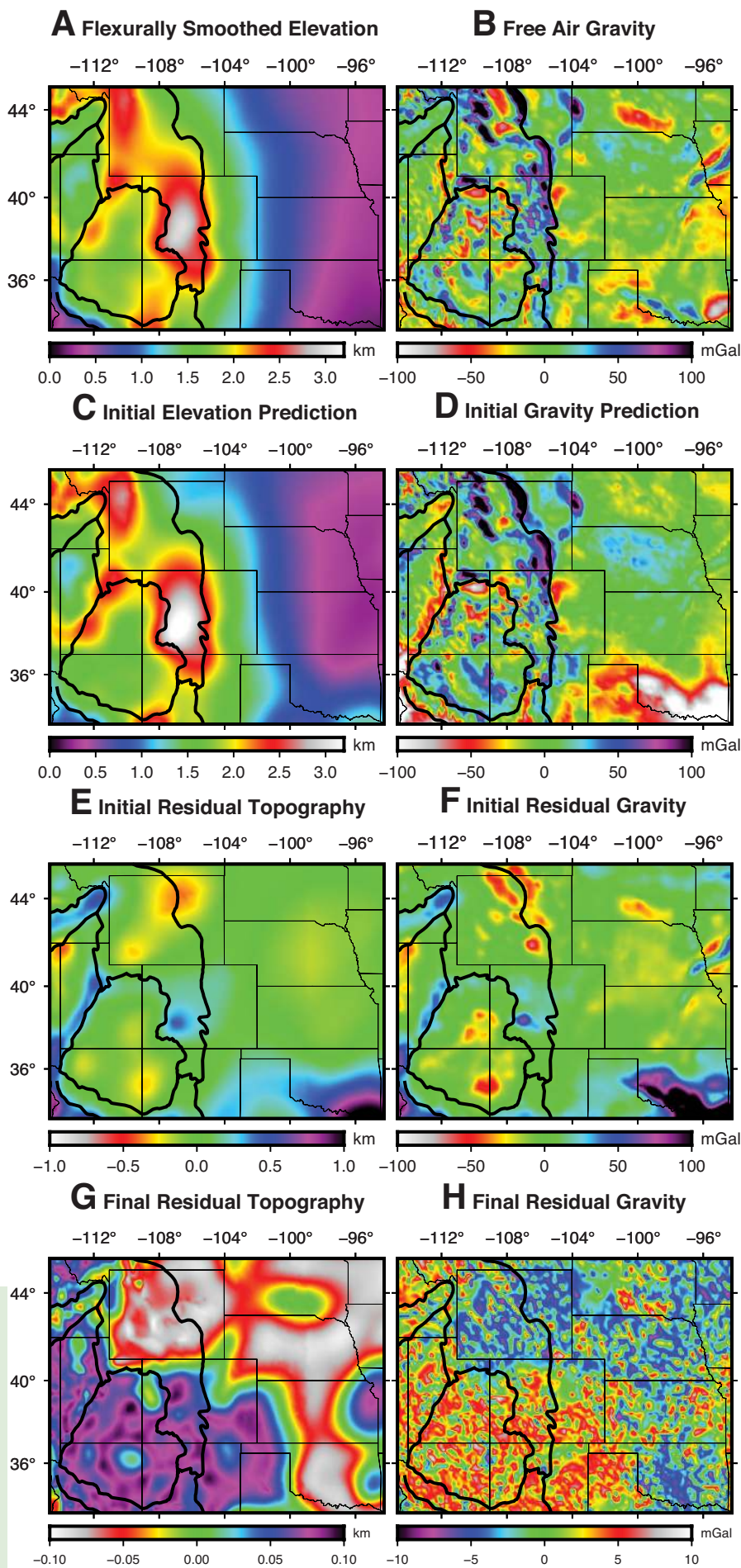


Figure 2. Gravity and topography maps. (A) Surface elevation (see Fig. 1A), smoothed by convolution with the flexural filter defined by lithospheric strength (here, using the elastic thickness model of Watts, 2012). Scale is the same as Fig. 1A. (B) Free-air gravity variations. The mean was removed because our method is chiefly sensitive to lateral variations in density. (C–D) Flexurally smoothed topography and gravity predicted by the initial density model (shown in Fig. 3). Scales as above. (E) Initial residual topography, defined as predicted minus observed elevation. Cool colors represent areas in which density must be greater than predicted; warm colors must be less dense. (F) Residual gravity, defined as observed minus predicted so that residuals generally have the same polarity as in E. Again, cool colors reflect underpredicted density. Residuals in E and F are generally small in magnitude and/or lateral extent compared to signals shown in A–B. (G–H) Final residuals associated with one of the 1000 Monte Carlo simulations.

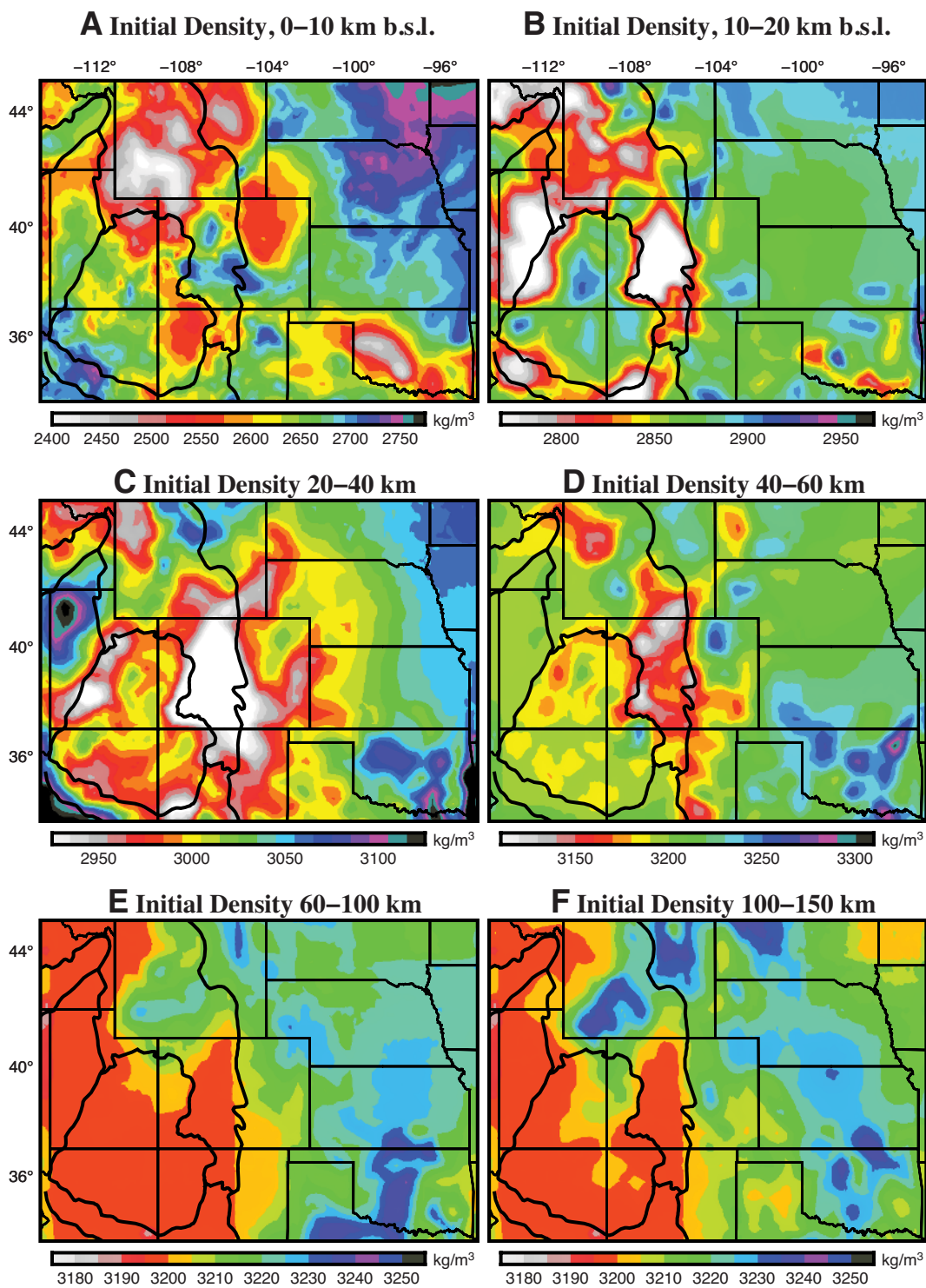


Figure 3. Initial density model, as derived from Equations 2–3. The median of 1000 simulations averaged over the listed depth intervals is shown.

the thermal velocity–density relation is depth dependent because of pressure- and period-dependent anelasticity.

The lithosphere was divided into 16 layers: surface to sea level, 12 layers of 5 km thickness from sea level to 60 km, and 30-km-thick layers from 60 to 150 km depth. The region was then divided into 20×20 km columns. Each cell ($20 \times 20 \times 5$ km above 60 km depth or $20 \times 20 \times 30$ km below) was assigned a uniform density, interpolated from the initial estimate from the randomly selected seismic velocity model of Shen et al. (2013) and Equations 2–3.

We then forward modeled gravity and flexurally smoothed topography (using the same procedure detailed by Levandowski et al., 2015) and compared the predictions of this initial model to observed gravity and flexurally smoothed surface elevation. To account for uncertainty in elastic thickness, each of the 1000 simulations randomly chose one of three two-dimensional elastic thickness models (Kirby and Swain, 2009; Lowry and Pérez-Gussinyé, 2011; Watts, 2012). We note, however, that the primary features that we discuss are suitably long-wavelength (>100 km) that the specific elastic thickness model has limited impact.

The velocity-density scaling reproduces the broad patterns of gravity and topography across the western United States (L1/L2 norms of 12.2/22.3 mGal and 124/155 m). Nevertheless, some short-wavelength gravity anomalies are unexplained, and there are modest misfits to topography (Figs. 2E–2F). Short-wavelength residuals may simply reflect features below the ~ 100 km resolution of the TA-derived models; considering gravity as well can sharpen images of lithospheric structure (e.g., Maceira and Ammon, 2009). Broader residuals plausibly reveal compositional variations in the mantle or crustal lithologies that do not conform to our velocity-density relation. For example, mantle melt depletion lowers density substantially and slightly increases S velocity (Lee, 2003; Schutt and Leshner, 2010): Assuming uniform composition, we would underestimate the elevation in areas with depleted mantle. Similarly, hydration (e.g., serpentinization) causes a greater loss in density than estimated from our velocity-density scaling (cf. Eq. 3 with figure 1 of Christensen, 2004). Finally, the crustal velocity-density regression (Eq. 2) systematically underestimates the density of mafic units and overestimates that of many felsic rocks, with misfits as large as ~ 170 kg/m³ possible for some lithologies (Levandowski et al., 2015).

In order to reproduce gravity and topography, as well as to improve lateral resolution of lithospheric structure, we next allowed departures from the initial density estimate. These departures essentially relaxed the assumptions of homogeneous mantle composition and of a fixed crustal velocity-to-density scaling, and allowed imaging of shorter-wavelength features.

Density Refinement

Density cannot be known from seismic velocity alone, for at least three reasons. (1) Our models seek finer-scale resolution than the ~ 100 km horizontal resolution of the velocity models derived from TA surface wave data. (2) There is uncertainty in the velocity models, which can be quantified in terms of the range of velocity at any given depth across the hundreds of acceptable velocity

models beneath any seismic station. (3) There simply is not a single-valued mapping of velocity to density that captures all lithologies or all chemical/compositional trends (e.g., melt depletion). Additional factors, such as Vp/Vs variations, departures from the Q model chosen by Shen et al. (2013), and anisotropy would also influence the conversion of Rayleigh wave phase velocities and receiver functions to velocity profiles, and the subsequent conversion of these models to density. Put differently, there are factors that affect seismic velocity but not density, factors that affect density but not velocity, and features of the density of the crust and upper mantle—with or without a seismic signature—that are simply finer than the velocity models can resolve. Patterns and biases that are of particular importance to the present study include melt depletion, serpentinization, and the bias of Equation 2 to systematically overestimate the density of felsic material and underestimate the density of mafic material, as discussed already.

The misfits between predictions of the initial density model and observed gravity and topography are generally small compared to the ~ 3 km of relief across the study area and the large variations in free-air gravity (Fig. 2). Nevertheless, to produce more robust density models, we employed the random walk Monte Carlo algorithm of Levandowski et al. (2015) to refine the initial density structures until the density model reproduced gravity and flexural topography to within 10 mGal and 100 m at all points in the study area. The Monte Carlo proceeds by selecting one of the nodes from the 20×20 km grid at random. A cell beneath that node and a density perturbation (limited to ± 150 kg/m³ in the crust and ± 50 kg/m³ in the mantle) are chosen at random, and the attendant variance reductions (or increases) of gravity and topography residuals are calculated. The algorithm is offered a number of cell/density-perturbation choices, initially two, but increasing in number through the inversion to aid convergence, and it ultimately selects the best-fitting one (even if that increases residual variance) and applies that change to the density of that cell, and updates residuals. When the model reproduces gravity and flexurally modulated topography to within 10 mGal and 100 m at all points in the study area, the 3-D density model is accepted as a member of a posterior distribution of acceptable density structures. This process—randomly selecting one of Shen’s models at each TA station, converting velocity to density, selecting one of three elastic thickness models, forward modeling gravity and flexural topography, and iteratively refining the density model—is repeated 1000 times to embrace the non-uniqueness of gravity and topography. Uncertainties of density models are discussed in the Supplemental Material (see footnote 1), but a typical uncertainty of density in a region is ~ 15 kg/m³.

The magnitude of the adjustments that are necessary to match gravity and topography (Fig. 4) average ~ 14 kg/m³ in the crust and 5 kg/m³ in the mantle, and adjustments are typically less than ~ 100 km in the lateral dimension. The crustal adjustments are small compared to the plausible range of ~ 170 kg/m³ that a rock of known velocity may have. Moreover, these adjustments are well within the uncertainties of the velocity models. Because Shen et al. (2013) provided as many as thousands (generally hundreds) of velocity models at each TA station, the velocity-derived uncertainty in density at any point is readily

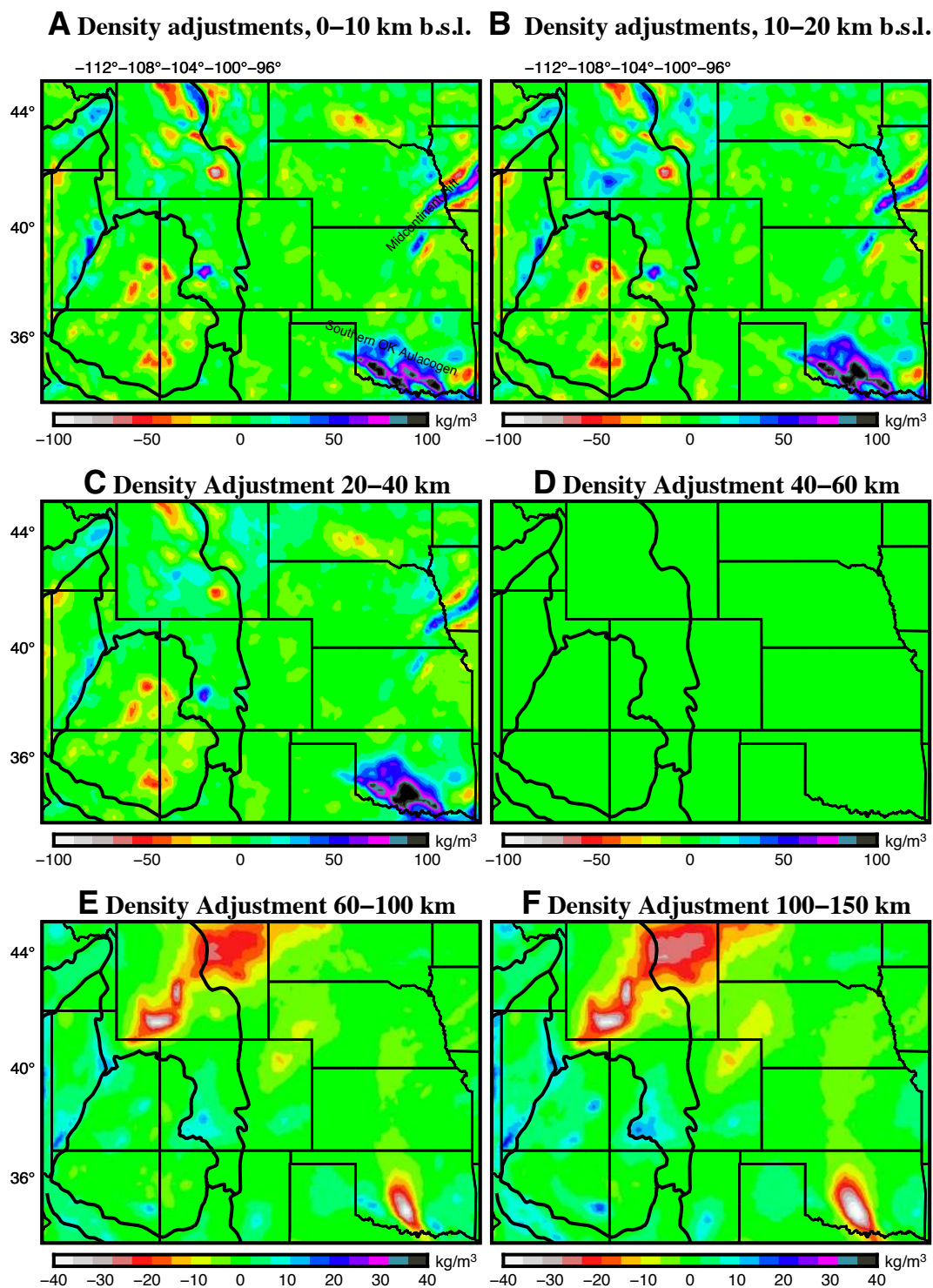


Figure 4. (A–F) Density adjustments, with the median value of 1000 simulations averaged over the listed depth intervals. These adjustments are inferred to represent structures below the lateral resolution of the seismic velocity models if less than ~100 km across or materials that do not conform to the assumptions that underlie Equations 2–3. The most prominent crustal features (A–C) are the positive density adjustments near mafic intrusions associated with the Midcontinent Rift and Oklahoma aulacogen. In the mantle lithosphere (E–F), negative density adjustments in the Wyoming craton may reflect melt depletion.

quantified. The range on either side of the median that subsumes 95% of their models is ~0.2 km/s in the midcrust and upper mantle, ~0.3 km/s in the lower crust, and greater still in the uppermost crust. As such, the inherent range of density estimated from those velocity models exceeds $\pm 100 \text{ kg/m}^3$ throughout the crust and is approximately $\pm 30 \text{ kg/m}^3$ in the mantle.

The two areas with large-magnitude and laterally extensive adjustments are an $\sim 300 \times 300 \text{ km}$ portion of the upper mantle beneath the Wyoming craton that is some 25 kg/m^3 less dense than estimated (Figs. 4E–4F) and an $\sim 100 \times 200 \text{ km}$ region near the Southern Oklahoma aulacogen in which the crust is $75\text{--}100 \text{ kg/m}^3$ denser than estimated (Figs. 4E–4F). These departures from the seismically derived density estimates are within the typical uncertainties associated with the velocity models themselves, but they could also represent systematic deviations from Equations 2–3 such as the compositional anomalies discussed earlier. In the Wyoming craton, we speculate that the low-density but high-velocity Archean mantle is melt-depleted residuum from the initial, high-temperature extraction of crustal material $>2 \text{ Ga}$. In southern Oklahoma, three lines of evidence suggest that very dense crust is likely partially eclogitized mafic intrusions. First, the anomaly lies in or near the Oklahoma aulacogen, which underwent extension and associated emplacement of mafic sills and dikes in the Eocambrian. The aulacogen was subsequently the focus of early-stage NE–SW Ouachita contraction, which would have thickened the suite of mafic units under horizontal compression. Second, it is the densest material in the study area but is above the receiver function–defined Moho. Third, it is denser than expected from Equation 2, which—as argued by Levandowski et al. (2015) for the northern portion of the Midcontinent Rift (Fig. 4A)—is a hallmark of mafic crustal lithologies.

■ HYPOTHESIS TESTS

Earlier herein, we enumerated the possible causes of Cenozoic uplift of the Colorado Plateau and western Great Plains relative to the eastern Great Plains. We now discuss the testable predictions that each hypothesis makes about seismic velocity and density structure. The simplest prediction that each hypothesis makes is where in the lithosphere modern topographic relief is supported. For example, arguments in favor of mantle heating would require that support for modern relief is derived from mantle depths. In addition to the depths of density variations, each hypothesis makes certain predictions about the relationships between velocity and density (i.e., the validity of Equations 2–3 and of our underlying assumptions, manifest as whether adjustments to our initial, seismically derived models are necessary).

Mantle Heating

Increases in average mantle temperature could either be conductive (e.g., Roy et al., 2009) or advective, such as lithospheric thinning and replacement

by warmer asthenosphere. One version of the former hypothesis—conductive reheating of unthinned lithosphere following a period of insulation by the Farallon slab—can be dismissed because such reheating does not account for any uplift relative to the Paleozoic–Mesozoic (i.e., before cooling). If Cenozoic lithospheric thinning caused differential uplift, however, the density of the lower lithosphere should decrease from east to west across the Great Plains and/or be less beneath the Colorado Plateau than the eastern Great Plains. Additionally, since our initial assumption is that mantle velocities reflect temperature variations, this systematic trend in mantle density should exist in our initial, seismically derived model.

Mantle Chemical or Phase Changes

In a region of substantially melt-depleted lithosphere, a velocity-temperature-density scaling should also lead to underpredicted elevations. Although xenoliths from the Colorado Plateau record upper mantle that is $\sim 1\%$ enriched in magnesium (Alibert, 1994; Lee et al., 2001), the predicted elevation in the Colorado Plateau and western Great Plains is generally well explained by our initial density models (Fig. 2), which consider only thermal variations. Moreover, melt depletion would have to have occurred during the Cenozoic, which is at odds with the paucity of volcanism in the Colorado Plateau and Great Plains.

Mantle hydration (e.g., serpentinization) is also recorded in some Colorado Plateau xenoliths (Usui et al., 2003; Smith and Griffin, 2005), but the effects of fluid flux on velocity and density depend on the specifics of its chemical and/or compositional impact. As noted above, serpentinization causes a proportionally greater decrease in density for a unit velocity decrease than predicted by Equation 3 (compare figure 1 of Christensen, 2004, with our Equations 3a and 3b); our initial density estimate would therefore be too great if substantial serpentinized material is present in the upper mantle. By contrast, incorporation of hydroxyl groups into nominally anhydrous olivine can have a strong impact on velocity, but unit cell volumes increase only slightly (Smyth and Jacobsen, 2006); in this case, our density estimate would be lower than the true density. Finally, fluid flux can deliver silica to the mantle lithosphere and possibly increase orthopyroxene at the expense of olivine, but this compositional trend has little effect on shear velocity or density (Schutt and Leshner, 2010). We argue against the first two possibilities because the mantle density beneath the Colorado Plateau and Great Plains accords so well with an estimate based on the assumption that velocity reflects temperature alone. Our models would be insensitive to the latter trend, but orthopyroxene enrichment is not correlated with density decrease anyway (Schutt and Leshner, 2010), so it would not explain uplift.

Although we argue against the three hydration-induced changes discussed here, many other effects of fluid flux are possible. It is crucial to note that any phenomenon that affects both velocity and density, and that does so in similar proportion to that derived in Equation 3 (i.e., with $\sim 6 \text{ kg/m}^3$ density change corresponding to 1% shear velocity change) would be incorrectly ascribed to temperature variations. In other words, our null hypothesis is that all velocity

variations reflect temperature variations. We test this hypothesis by scaling velocity to density using a thermal relationship, and then comparing predicted and observed gravity and topography. Because observations are reproduced rather well, we do not question the null hypothesis further, but we do acknowledge that if another factor controls velocity and density and produces a similar relationship to that described by Equation 3, our simple test would cause us to wrongly accept the hypothesis that mantle velocity and density variations are primarily functions of temperature variations.

Crustal Phase Changes

Midcrustal xenoliths from the Navajo volcanic field on the Colorado Plateau record hydration-induced retrogression of garnet-bearing crustal assemblages to less dense mineralogies. Th-Pb dating of secondary monazite associated with these assemblages suggests that the majority of the retrogression occurred in the latest Cretaceous (Butcher, 2013; Butcher et al., 2017), contemporaneous with the arrival of the Farallon slab. A similar but undated retrograde reaction is documented in crustal xenoliths near the northern Great Plains: Southward from near the Canadian border to southern Wyoming, three xenolith localities increase in elevation from 1 to 2.5 km as xenolith density decreases by $\sim 500 \text{ kg/m}^3$ (Barnhart et al., 2012; Farmer et al., 2012; Mahan et al., 2012). Noting a collocated southward decrease in seismic velocity in an ~ 10 -km-thick layer of lower crust, Jones et al. (2015) hypothesized (following Eq. 1) that hydration-induced retrogression produced much of the modern relief on the Great Plains. If so, then it follows that the modern density of the lower crust should decrease systematically from east to west. Additionally, the xenoliths discussed by Jones et al. (2015) and Butcher et al. (2017) have P-velocity-density trends that are broadly concordant with that of the lithologies used to develop Equation 2. Therefore, it is possible that such an east-west gradient in density would be manifest in velocities as well, though shear-velocity measurements are not available for those xenoliths. We discuss lower-crustal hydration specifically, but we note that any other mechanism of broad, dedensifying phase changes might produce similar patterns.

Dynamic Topography

If surface elevation in a region were sustained by asthenospheric flow rather than lithospheric buoyancy (Moucha et al., 2008; Liu and Gurnis, 2010), seismic velocity would generally reflect the density of the crust and upper mantle: The predicted gravity would match observations, but such a region would stand at greater elevation than predicted. This pattern is not revealed by the residuals shown in Figure 2 in either the Colorado Plateau or the western Great Plains, where the initial model generally reproduces modern elevation. Therefore, we suggest that the impact of asthenospheric flow is minimal, perhaps <100 m. There is an important distinction between flow and density,

however. We did not explicitly separate lithosphere and asthenosphere, and we included sublithospheric loads into our flexural-isostatic buoyant heights. We did indeed find modest variations in density at depths that likely correspond to asthenosphere, but we refer to any potential dynamic component as non-isostatic forces related to flow itself. Recently, Afonso et al. (2016) reached a similar conclusion—that dynamic topography is of secondary importance—even though their modeling explicitly calculated the vertical normal stress imparted on the base of the lithosphere by both the buoyancy/antibuoyancy of sublithospheric loads and by buoyancy-induced flow.

■ CAUSES OF CENOZOIC DIFFERENTIAL UPLIFT

Great Plains: Lower-Crustal Hydration

After accounting for the east-to-west increase in the thickness of Cretaceous sediments, a nearly linear increase in elevation across the Great Plains—more than 800 m at the Rocky Mountain front—remains unexplained. Our modeling reveals that the density of the lower crust—averaged longitudinally—decreases systematically from east to west. Little systematic difference is seen at other depths, casting doubt on the role of midcrustal alteration or mantle processes in supporting modern topographic slope. The average lower-crustal density (20–45 km) is 112 kg/m^3 less in the western Great Plains than in the eastern Great Plains (Fig. 5), supporting ~ 900 m of modern surface relief (Fig. 1B). Thus, density variations in the lower crust combine with Cenozoic sedimentation to account almost exactly for Cenozoic differential uplift across the Great Plains. Of the potential causes of uplift, crustal hydration is most consistent with this pattern, speculatively reflecting progressive dewatering of the Farallon slab with distance eastward under North America.

Finding, not surprisingly, a similar pattern in lower-crustal density, Levandowski et al. (2017) suggested that the lowest densities may coincide with Proterozoic continental sutures (the Cheyenne belt—the suture between the Wyoming craton and Yavapai terranes—in SE Wyoming and the Yavapai-Mazatzal suture in SE Colorado). If so, it is reasonable to expect that fluids may preferentially exploit these preexisting, lithospheric-scale fracture/suture zones, and lower-crustal hydration may consequently be greatest there. In fact, studies of hydrated mantle xenoliths in the Colorado Plateau indicate that fluid flow is controlled by the presence of fractures (Nielson et al., 1993). Although this line of reasoning presents an internally consistent explanation for the heterogeneous lower crust of the western Great Plains, there is little agreement on the location and nature of Proterozoic sutures on the Great Plains. The Cheyenne belt is the topic of comparatively less debate, but the Yavapai-Mazatzal suture as sketched by Levandowski et al. (2017)—based on Carlson (2007)—is near the northern edge of the suture zone depicted by Whitmeyer and Karlstrom (2007) and is substantially north of the location given by Magnani et al. (2004). Thus, the details of lower-crustal density structure provide—at best—speculative additional evidence in favor of lower-crustal hydration, specifically

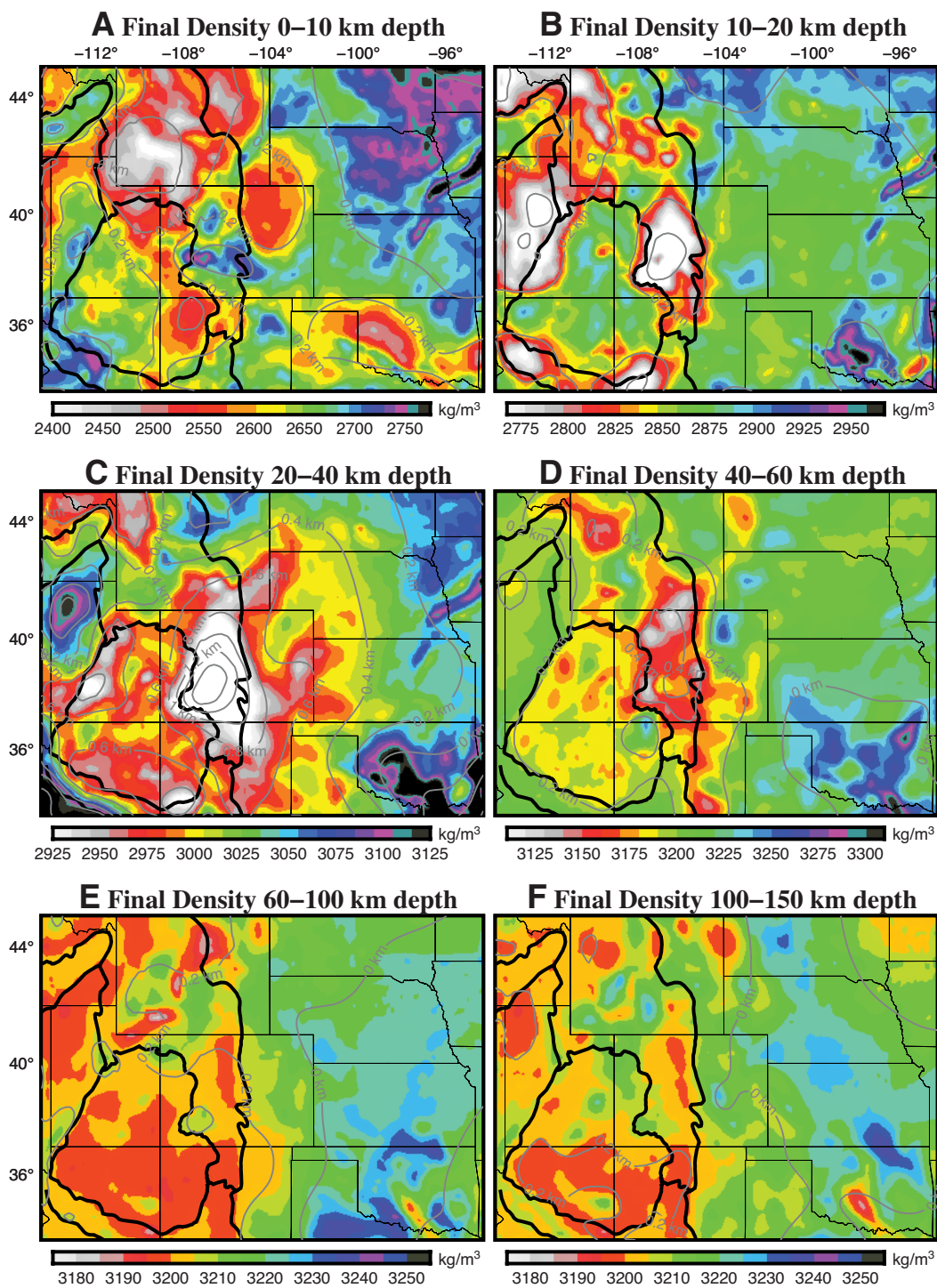


Figure 5. Final density model, the median of 1000 simulations averaged over the listed depth intervals. Contour lines note the flexurally modulated relief relative to the eastern Great Plains due to each depth range, with 0.2 km contour interval.

via the possibility that preexisting suture zones served as comparatively more efficient conduits for mantle-derived fluids than did intervening terranes.

Our purpose in this work was to investigate the broad-scale uplift of the Great Plains and Colorado Plateau. We argue that sedimentation and lower-crustal phase changes explain nearly all of the longitudinally averaged uplift. Smaller-scale topographic features may reflect other processes. For example, low-density mantle near the Jemez Lineament in northeastern New Mexico and southeastern Colorado supports ~500 m of uplift relative to the eastern Great Plains (Fig. 3). It is compelling to note that this area also stands 200–600 m higher (up to 2200 m; Fig. 1A) than most of the rest of the western Great Plains (Fig. 1), perhaps providing evidence in favor of mantle-derived uplift (Nereson et al., 2013). We conclude that second-order topographic features may reflect other mechanisms of support, but the broad difference between the western and eastern Great Plains arises from sedimentation and lower-crustal density.

Colorado Plateau: Lower-Crustal Hydration

Between 20 and 40 km depth, the Colorado Plateau averages 106 kg/m^3 less dense than the eastern Great Plains (Fig. 5), supporting 660 m of relief (Fig. 1B). As discussed earlier, there is likely some contribution from higher temperatures in the Colorado Plateau; following the same line of logic, we would estimate a $250 \text{ }^\circ\text{C}$ temperature anomaly at the Moho ($\sim 21 \text{ kg/m}^3$) and a $\sim 125 \text{ }^\circ\text{C}$ temperature anomaly at 20 km depth ($\sim 10.5 \text{ kg/m}^3$). Thus, the 20–40 km depth range may average 15 kg/m^3 less dense beneath the Colorado Plateau than the eastern Great Plains because of its temperature, but the remaining 91 kg/m^3 difference is better explained by compositional changes.

In addition, the 40–50 km depth range essentially subsumes the crust-mantle transition (Gilbert, 2012; Shen et al., 2013), and receiver functions generally image a gradient or low contrast in impedance across the Moho in the Colorado Plateau. The density of this transition zone is 55 kg/m^3 lower than at the same depths beneath the eastern Great Plains, and this explains an additional 170 m of differential Cenozoic uplift. After accounting for sedimentation and the effects of lower-crustal density loss, only 400 m of Colorado Plateau uplift remain.

Colorado Plateau: Lithospheric Thinning

The Colorado Plateau mantle is similar in density to that of the southern Rockies and Basin and Range and accommodates ~400 m of topographic relief relative to the eastern Great Plains (Fig. 1B). We infer that this density structure is thermal in origin (i.e., the Rockies, Colorado Plateau, and Basin and Range have warmer mantle than the Great Plains) because of the close correspondence between the elevation and gravity predicted by our thermal relation between velocity and density (Eq. 3) and observation. More obvious evidence

comes from the elevated Moho temperatures in the Colorado Plateau relative to the Great Plains (Afonso et al., 2016; Schutt et al., 2018). We do not explicitly distinguish between lithospheric mantle and asthenosphere, so higher temperatures could reflect thinner lithosphere or warmer lithosphere; if the lithosphere and asthenosphere are in thermal equilibrium, the two are likely intertwined, because convectively thinned lithosphere will subsequently warm. A Cenozoic increase in mantle temperature is therefore a possible source of Colorado Plateau uplift, but we have already discounted purely conductive heating, so we now focus on advective heating.

Advective heating may occur by removal of mantle lithosphere and its replacement with asthenosphere or by intrusion. Limited volcanic activity and intrusive activity, as well as crustal thickness estimates, are at odds with large-magnitude igneous intrusion, so we suggest lithospheric thinning. A sinking Rayleigh-Taylor instability (Levander et al., 2011), delamination (Bird, 1979), or ablation by the Farallon slab (Bird, 1988) could thin the lithosphere; we do not explicitly discriminate among these. Additionally, we did find some heterogeneity in density of the Colorado Plateau mantle, with comparatively higher density in the north-central portion, lower density around the margins, and the lowest densities in the south (Figs. 5E–5F). Heating/thinning of the Colorado Plateau lithosphere is likely heterogeneous, as also evidenced by encroachment of volcanism from the edges (Roy et al., 2009), but we will illustrate the effects of lithospheric thinning with 1-D thermal models meant to be reflective of the average across the Colorado Plateau. Because buoyancy changes are convolved with the flexural response of the lithosphere (and the Colorado Plateau lithosphere is comparatively strong, with elastic thickness ~30 km: Kirby and Swain, 2009; Lowry and Pérez-Gussinyé, 2011; Watts, 2012), it is indeed the average change in mantle buoyancy that is of interest to our present aim.

If the Mesozoic Colorado Plateau did indeed resemble the modern eastern Great Plains, the lithosphere would originally have been 150–200 km thick (van der Lee and Nolet, 1997; Yuan et al., 2014). In addition, if only the lower-mantle lithosphere was removed, then remaining melt-depleted material could later be sampled in xenolith suites (as argued by Spencer, 1996).

To estimate how much lithospheric thinning would be required in order to produce 400 m of modern uplift, we solved non-steady-state heat-transfer equations similar to those presented by Bird (1979). In that conception, a portion of lithosphere is removed at time 0 and replaced with uniform-temperature asthenosphere. The replacing material then remains fixed in space and cools conductively, essentially becoming thermal lithosphere. Here, we revisited this modeling and also solved similar non-steady-state heat-flow equations for the end-member situation that after lithospheric thinning, the replacing material does not cool off but rather is maintained convectively at a constant temperature, such that the lithosphere is permanently thinned. The former setup ignores convection, but the latter requires a long-term change in heat flux; neither is a perfect formulation. We view the two conceptions as bounding the reality that lies somewhere between these two idealizations.

Whatever the boundary conditions, the lithosphere (with thickness z_{old}) begins in equilibrium with asthenosphere of temperature $T_a = 1350$ °C, and the surface temperature is a constant $T_s = 20$ °C. At time $t = 0$, the lithosphere is thinned to a thickness z_{new} . If we also assume an initially linear geotherm, the temperature distribution immediately after removal is piecewise continuous:

$$T(z,0+) = T_s + (T_a - T_s)z/z_{old}, \text{ where } 0 \leq z < z_{new};$$

$$T(z,0+) = T_a \text{ where } z \geq z_{new}. \tag{4}$$

If the asthenosphere cools as a semi-infinite conductive half-space (essentially becoming thermal lithosphere), the temperature profile returns to a linear geotherm from the surface ($T = T_s$) to z_{old} ($T = T_a$). If the lithosphere thins

permanently, temperatures approach a steeper geotherm from the surface ($T = T_s$) to z_{new} ($T = T_a$).

For either case, the temperature as a function of depth and time can be calculated by separation of variables wherein the temperature profile is the sum of the steady-state temperature, $v(z)$, and a transient (decaying) perturbation, $w(z,t)$, to that temperature:

$$T(z,t) = v(z) + w(z,t). \tag{5}$$

The Fourier expansion of Equation 5 is (Boyce and DiPrima, 2003):

$$T(z,t) = v(z) + \sum_{n=1}^{\infty} c_n e^{-\frac{n^2\pi^2\kappa t}{L^2}} \sin \frac{n\pi z}{L}; c_n = \frac{2}{L} \int_0^L w(z, 0) \sin \frac{n\pi z}{L} dz. \tag{6}$$

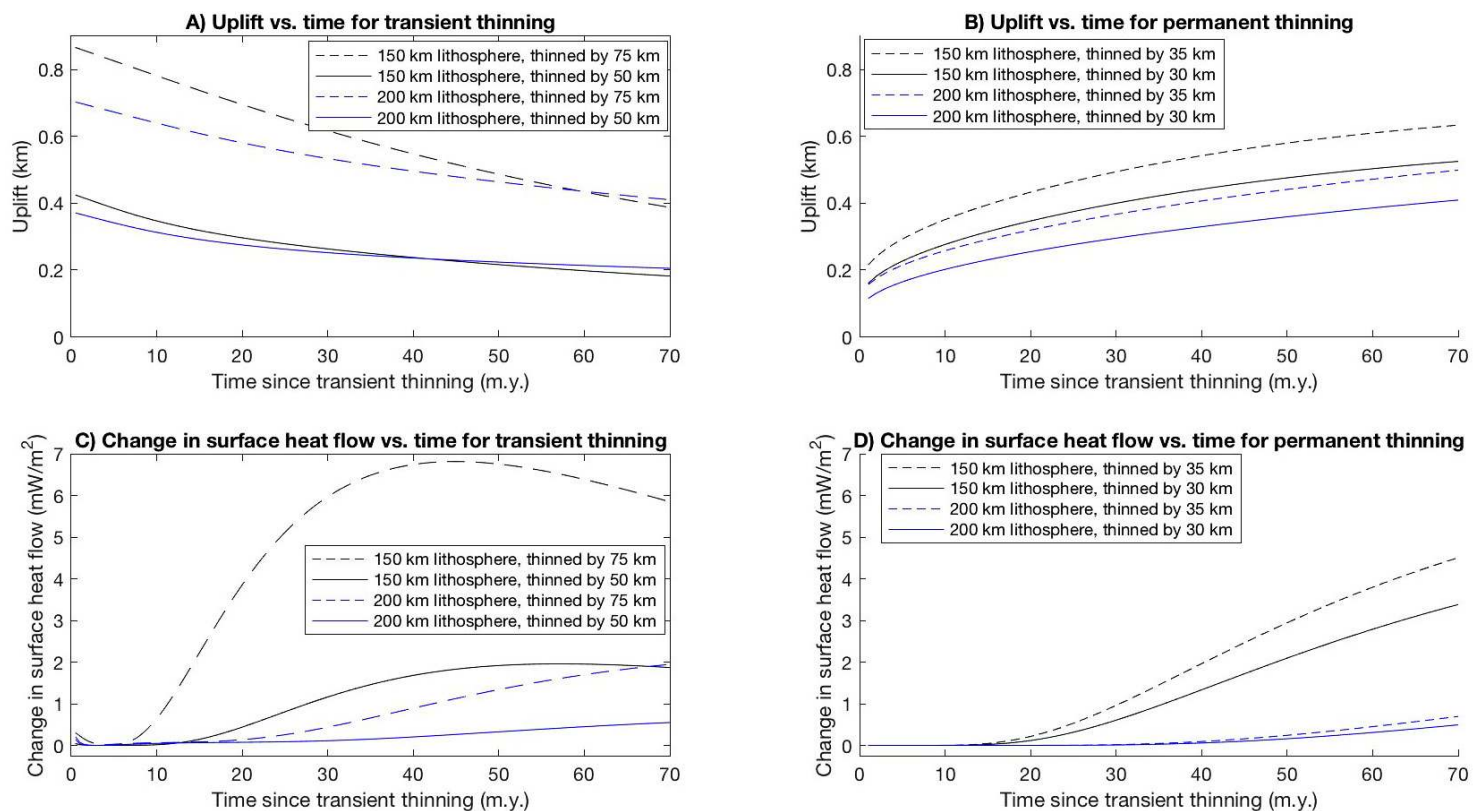


Figure 6. Uplift and change in surface heat flow as a function of time for transient and permanent thinning end-member boundary conditions and for 150 km and 200 km initial thicknesses of the lithosphere. Scenarios similar to those discussed in the text are shown (e.g., as shown by dashed lines in S3A, if either 200-km-thick or 150-km-thick lithosphere had thinned by 75 km at 70 Ma, 400 m of uplift would persist).

Here, L is the depth of the future conductive boundary (z_{new} or z_{old}), and $w(z,0) = T(z,0) - v(z)$. The thermal diffusivity, κ , is $1 \text{ mm}^2/\text{s}$.

Following Equation 1, the uplift as a function of time is proportional to the integrated change in temperature from the initial state (at $t < 0$):

$$U_{\text{total}}(t, L, z_{\text{old}}) = \alpha L \int_0^{z_{\text{old}}} (T(z, t) - T(z, 0)) dz. \quad (7)$$

The final unknowns are the initial lithospheric thickness—we used plausible values of 150 and 200 km, based on estimates of the modern eastern Great Plains (van der Lee and Nolet, 1997; Yuan et al., 2014)—and when thinning occurred. Figures 6A and 6B show a number of uplift versus time curves. (We used a constant coefficient of thermal expansion, α , of $3.2 \times 10^{-5}/^\circ\text{C}$.) If the lithosphere thins permanently, initial uplift is followed by a protracted period of asymptotic, ongoing surface uplift. If the replacing material cools, the elevation gain will decay away. Since there is no discernible heat flow anomaly in the modern Colorado Plateau, we also checked the predicted change in surface heat flow from each model (quantified as $k[T_{5\text{km}} - T_s]/5$, where $k = 3 \text{ mW m}^{-2}^\circ\text{C}^{-1}$), shown in Figures 6C and 6D. The change for all models that produced 400 m of modern uplift relative to the initial state is a few milliwatts per square meter, which is allowed by observations. We next calculated the depth of the lithosphere-asthenosphere boundary immediately after thinning and the amount of lithospheric thinning needed to produce ~400 m of modern uplift for the various scenarios (transient vs. permanent thinning and initial lithospheric thickness of 150 vs. 200 km) for thinning at 70 Ma (the arrival of the Farallon slab), 30 Ma (slab rollback/the ignimbrite flare-up), and 0 Ma (Figs. 7A–7B).

All acceptable scenarios left most of the mantle lithosphere intact to later be sampled as magnesian xenoliths (Alibert, 1994; Lee et al., 2001). Transient thinning required 45–70 km of lithosphere to be removed; permanent thinning required 25–50 km (Fig. 7B). Thus, we suggest that the Colorado Plateau and the western Great Plains experienced similar amounts of lower-crustal hydration by fluids exsolved from the Farallon slab, but the lithosphere beneath the Colorado Plateau also thinned by a few tens of kilometers during the Cenozoic, causing an additional 400 m of uplift.

Because the removal of mantle lithosphere by Rayleigh-Taylor instability, delamination, or similar mechanisms should create a number of small-scale convection cells, a more appropriate treatment of the problem might hold the lithosphere-asthenosphere boundary at a constant temperature for some time before allowing the replacing asthenosphere to begin to cool. The differential equations required to solve such a problem are the same as Equations 4–7. We conducted many trials with varying durations of what is effectively forced convection, and even a comparatively short duration of the constant-temperature-asthenosphere phase greatly protracted uplift and decreased the amount of thinning necessary. As such, the true amount of lithospheric thinning and the thickness of remaining lithosphere are likely closer to the permanent thinning case, <50 km.

An additional set of calculations was performed (not shown) to determine the effect of a period of refrigeration of the overlying lithosphere. Specifically

(e.g., as posited by Roy et al., 2009), a shallowly subducting slab would isolate the base of the lithosphere from asthenospheric convection and cause the lithosphere to cool, densify, and subside. We find that even 20 m.y. of refrigeration (150-km-deep lithosphere-asthenosphere boundary cooled from 1350°C to 900°C and held fixed for 20 m.y.) would only produce ~250 m of thermal subsidence. Since we also posit that the cooled lower portion of the lithosphere was removed, if thinning occurred after or as the slab was removed, the effect on surface topography would be inconsequential.

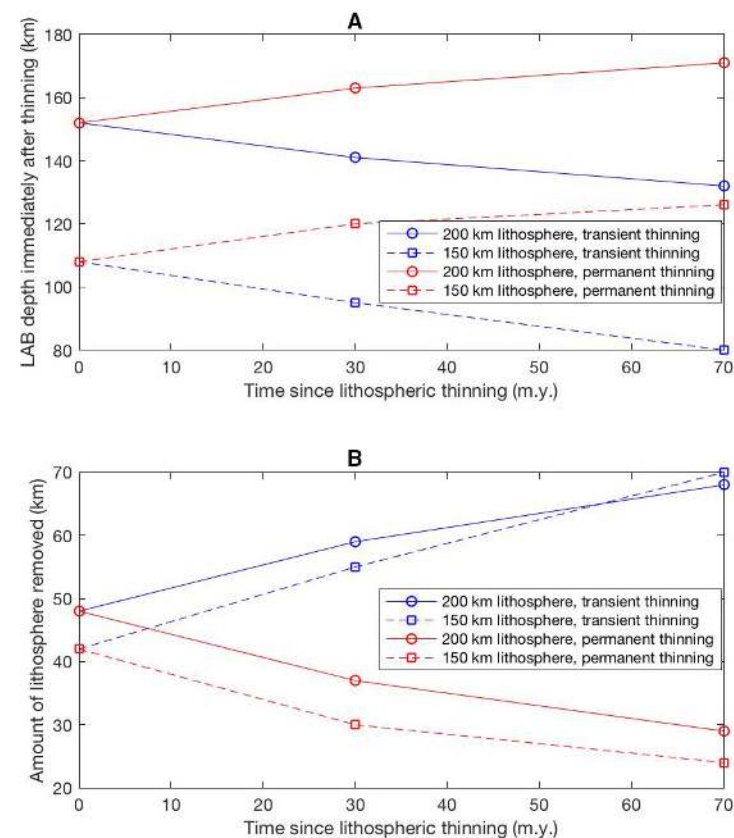


Figure 7. (A–B) Results of non-steady-state thermal models. For a given time since lithospheric thinning and initial thickness (either 150, dashed lines, or 200 km, solid lines), we solved for the amount of lithosphere that must have been removed under both constant-heat-flux boundary conditions (i.e., conductive heat transfer and thus transient thinning; blue lines) and constant asthenospheric temperature (i.e., purely convective heat transfer below the lithosphere and thus permanent thinning; red lines). Some 25–70 km of material must have been removed (B). The thickness of preserved mantle lithosphere is 80–180 km (A). Consequently, melt-depleted mantle lithosphere may remain beneath the Colorado Plateau, as known from xenoliths. LAB—lithosphere-asthenosphere boundary.

CONCLUSION

Cenozoic uplift of the largely undeformed Colorado Plateau and Great Plains was mainly achieved by hydration-induced retrogression of the lower crust by Farallon slab-derived fluids and accumulation of sediments during the Cretaceous and Early Tertiary. The 1.3 km of differential Cenozoic uplift across the Great Plains is due in part to an east-west gradient in the thickness of post-Jurassic sediments, which supports 0.4 km. A separate decrease in lower-crustal density, which can be explained by hydration due to mantle-derived fluids, caused the remaining 900 m. Of the 1.6 km of relative uplift of the Colorado Plateau, 250 and 950 m can be ascribed to sedimentation and lower-crustal hydration, respectively, and the final 400 m most plausibly resulted from Cenozoic removal of the lower 25–70 km of the mantle lithosphere.

ACKNOWLEDGMENTS

We thank Derek Schutt, Juan Carlos Afonso, and an anonymous reviewer for their comments. Mahan received funding from National Science Foundation grants EAR-0746246 and EAR-1053291. The development of the density modeling algorithm was funded by a Mendenhall Postdoctoral Fellowship to Levandowski.

REFERENCES CITED

- Afonso, J.C., Ranalli, G., and Fernández, M., 2005, Thermal expansivity and elastic properties of the lithospheric mantle: Results from mineral physics of composites: *Physics of the Earth and Planetary Interiors*, v. 149, no. 3–4, p. 279–306, <https://doi.org/10.1016/j.pepi.2004.10.003>.
- Afonso, J.C., Rawlinson, N., Yang, Y., Schutt, D.L., Jones, A.G., Fullea, J., and Griffin, W.L., 2016, 3-D multiobservable probabilistic inversion for the compositional and thermal structure of the lithosphere and upper mantle: III. Thermochemical tomography in the western-central U.S.: *Journal of Geophysical Research*, v. 121, p. 7337–7370, <https://doi.org/10.1002/2016JB013049>.
- Alibert, C., 1994, Peridotite xenoliths from western Grand Canyon and The Thumb: A probe into the subcontinental mantle of the Colorado Plateau: *Journal of Geophysical Research—Solid Earth*, v. 99, p. 21,605–21,620, <https://doi.org/10.1029/94JB01555>.
- Barnhart, K.R., Mahan, K.H., Blackburn, T.J., Bowring, S.A., and Dudas, F.O., 2012, Deep crustal xenoliths from central Montana, USA: Implications for the timing and mechanisms of high-velocity lower crust formation: *Geosphere*, v. 8, no. 6, p. 1408–1428, <https://doi.org/10.1130/GES00765.1>.
- Bird, P., 1979, Continental delamination and the Colorado Plateau: *Journal of Geophysical Research—Solid Earth*, v. 84, p. 7561–7571, <https://doi.org/10.1029/JB084iB13p07561>.
- Bird, P., 1984, Laramide crustal thickening event in the Rocky Mountain foreland and Great Plains: *Tectonics*, v. 3, no. 7, p. 741–758, <https://doi.org/10.1029/TC003i007p0741>.
- Bird, P., 1988, Formation of the Rocky Mountains, western United States: A continuum computer model: *Science*, v. 239, no. 4847, p. 1501–1507, <https://doi.org/10.1126/science.239.4847.1501>.
- Blackwell, D.D. and Richards, M., eds., 2004, *Geothermal Map of North America*, <https://www.smu.edu/Dedman/Academics/Programs/GeothermalLab/DataMaps>.
- Blackwell, D., Richards, M., Frone, Z., Ruzo, A., and Dingwall, R., 2011, Temperature-at-depth maps for the conterminous US and geothermal resource estimates: *Geothermal Resources Council (GRC) Transactions*, v. 35, p. 1545–1550.
- Bouhifd, M.A., Andraut, D., Fiquet, G., and Richet, P., 1996, Thermal expansion of forsterite up to the melting point: *Geophysical Research Letters*, v. 23, no. 10, p. 1143–1146, <https://doi.org/10.1029/96GL01118>.
- Boyce, W.E., and DiPrima, R.C., 2003, *Elementary Differential Equations and Boundary Value Problems*: New York, Wiley, 759 p.
- Brocher, T.M., 2005, Empirical relations between elastic wavespeeds and density in the Earth's crust: *Bulletin of the Seismological Society of America*, v. 95, no. 6, p. 2081–2092, <https://doi.org/10.1785/0120050077>.
- Butcher, L.A., 2013, *Rethinking the Laramide: Investigating the Role of Fluids in Producing Surface Uplift Using Xenolith Mineralogy and Geochronology* [M.S. thesis]: Boulder, Colorado, University of Colorado, 79 p.
- Butcher, L.A., Mahan, K.H., and Allaz, J.M., 2017, Late Cretaceous crustal hydration in the Colorado Plateau, USA, from xenolith petrology and monazite geochronology: *Lithosphere*, v. 9, no. 4, p. 561–578, <http://doi.org/10.1130/L583.1>.
- Carlson, M.P., 2007, Precambrian accretionary history and Phanerozoic structures—A unified explanation of tectonic features of the Nebraska region, USA, in Hatcher, R.D., Jr., Carlson, M.P., McBride, J.H., and Martínez Catalán, J.R., eds., 4-D Framework of Continental Crust: *Geological Society of America Memoir* 200, p. 321–326, [https://doi.org/10.1130/2007.1200\(15\)](https://doi.org/10.1130/2007.1200(15)).
- Christensen, N.I., 1996, Poisson's ratio and crustal seismology: *Journal of Geophysical Research—Solid Earth* (1978–2012), v. 101, no. B2, p. 3139–3156, <http://doi.org/10.1029/95JB03446>.
- Christensen, N.I., 2004, Serpentinites, peridotites, and seismology: *International Geology Review*, v. 46, p. 795–816, <https://doi.org/10.2747/0020-6814.46.9.795>.
- Cook, T.D., and Bally, A.W., 1975, *Stratigraphic Atlas of North America*: Princeton, New Jersey, Princeton University Press, 280 p.
- Davis, G.H., 1978, Monocline fold pattern of the Colorado Plateau, in Matthews, V., III, ed., *Laramide Folding Associated with Basement Block Faulting in the Western United States*: *Geological Society of America Memoir* 151, p. 215–234.
- Farmer, G.L., Bowring, S.A., Williams, M.L., Christensen, N.I., Matzel, J.P., and Stevens, L., 2012, Contrasting lower crustal evolution across an Archean–Proterozoic suture: Physical, chemical and geochronologic studies of lower crustal xenoliths in southern Wyoming and northern Colorado, in Karlstrom, K.E., and Keller, G.R., eds., *The Rocky Mountain Region: An Evolving Lithosphere: Tectonics, Geochemistry, and Geophysics*: *American Geophysical Union Geophysical Monograph* 154, p. 139–162.
- Gilbert, H., 2012, Crustal structure and signatures of recent tectonism as influenced by ancient terranes in the western United States: *Geosphere*, v. 8, p. 141–157, <https://doi.org/10.1130/GES00720.1>.
- Hugh-Jones, D., 1997, Thermal expansion of MgSiO₃ and FeSiO₃ ortho- and clinopyroxenes: *The American Mineralogist*, v. 82, p. 689–696, <https://doi.org/10.2138/am-1997-7-806>.
- Jackson, I., and Faul, U.H., 2010, Grain size-sensitive viscoelastic relaxation in olivine: Towards a robust laboratory-based model for seismological application: *Physics of the Earth and Planetary Interiors*, v. 183, no. 1–2, p. 151–163, <https://doi.org/10.1016/j.pepi.2010.09.005>.
- Jackson, J.M., Palko, J.W., Andraut, D., Sinogeikin, S.V., Lakshtanov, D.L., Wang, J., Bass, J.D., and Zha, C.-S., 2003, Thermal expansion of natural orthoenastatite to 1473 K: *European Journal of Mineralogy*, v. 15, no. 3, p. 469–473, <https://doi.org/10.1127/0935-1221/2003/0015-0469>.
- Jones, C.H., Mahan, K.H., Butcher, L.A., Levandowski, W.B., and Farmer, G.L., 2015, Continental uplift through crustal hydration: *Geology*, v. 43, p. 355–358, <https://doi.org/10.1130/G36509.1>.
- Kirby, J.F., and Swain, C.J., 2009, A reassessment of spectral Te estimation in continental interiors: The case of North America: *Journal of Geophysical Research—Solid Earth* (1978–2012), v. 114, no. B8, B08401, <https://doi.org/10.1029/2009JB006356>.
- Lachenbruch, A.H., and Morgan, P., 1990, Continental extension, magmatism and elevation; Formal relations and rules of thumb: *Tectonophysics*, v. 174, no. 1–2, p. 39–62, [https://doi.org/10.1016/0040-1951\(90\)90383-J](https://doi.org/10.1016/0040-1951(90)90383-J).
- Lee, C.T., Yin, Q., Rudnick, R.L., and Jacobsen, S.B., 2001, Preservation of ancient and fertile lithospheric mantle beneath the southwestern United States: *Nature*, v. 411, p. 69–73, <https://doi.org/10.1038/35075048>.
- Lee, C.-T.A., 2003, Compositional variation of density and seismic velocities in natural peridotites at STP conditions: Implications for seismic imaging of compositional heterogeneities in the upper mantle: *Journal of Geophysical Research—Solid Earth*, v. 108, p. 2441, <https://doi.org/10.1029/2003JB002413>.
- Levander, A., Schmandt, B., Miller, M.S., Liu, K., Karlstrom, K.E., Crow, R.S., Lee, C.T.A., and Humphreys, E.D., 2011, Continuing Colorado Plateau uplift by delamination-style convective lithospheric downwelling: *Nature*, v. 472, no. 7344, p. 461–465, <https://doi.org/10.1038/nature10001>.
- Levandowski, W., and Jones, C.H., 2015, Linking Sierra Nevada, California, uplift to subsidence of the Tulare Basin using a seismically derived density model: *Tectonics*, v. 34, no. 11, p. 2349–2358, <https://doi.org/10.1002/2015TC003824>.

- Levandowski, W., Jones, C.H., Reeg, H., Frassetto, A., Gilbert, H., Zandt, G., and Owens, T.J., 2013, Seismological estimates of means of isostatic support of the Sierra Nevada: *Geosphere*, v. 9, no. 6, p. 1552–1561, <https://doi.org/10.1130/GES00905.1>.
- Levandowski, W., Boyd, O., Briggs, R., and Gold, R., 2015, A random-walk algorithm for modeling lithospheric density and the role of body forces in the evolution of the Midcontinent Rift: *Geochemistry, Geophysics, Geosystems*, v. 16, p. 4084–4107, <https://doi.org/10.1002/2015GC005961>.
- Levandowski, W., Zellman, M., and Briggs, R., 2017, Gravitational body forces focus North American intraplate earthquakes: *Nature Communications*, v. 8, 14314, <https://doi.org/10.1038/ncomms14314>.
- Liu, L., and Gurnis, M., 2010, Dynamic subsidence and uplift of the Colorado Plateau: *Geology*, v. 38, no. 7, p. 663–666, <https://doi.org/10.1130/G30624.1>.
- Lowry, A.R., and Pérez-Gussinyé, M., 2011, The role of crustal quartz in controlling Cordilleran deformation: *Nature*, v. 471, no. 7338, p. 353–357, <https://doi.org/10.1038/nature09912>.
- Maceira, M., and Ammon, C.J., 2009, Joint inversion of surface wave velocity and gravity observations and its application to central Asian basins shear velocity structure: *Journal of Geophysical Research–Solid Earth*, v. 114, B02314, <https://doi.org/10.1029/2007JB005157>.
- Magnani, M.B., Miller, K.C., Levander, A., and Karlstrom, K., 2004, The Yavapai–Mazatzal boundary: A long-lived tectonic element in the lithosphere of southwestern North America: *Geological Society of America Bulletin*, v. 116, p. 1137–1142, <https://doi.org/10.1130/B25414.1>.
- Mahan, K.H., Schulte Pelkum, V., Blackburn, T.J., Bowering, S.A., and Dudas, F.O., 2012, Seismic structure and lithospheric rheology from deep crustal xenoliths, central Montana, USA: *Geochemistry, Geophysics, Geosystems*, v. 13, Q10012, <https://doi.org/10.1029/2012GC004332>.
- McGetchin, T.R., Burke, K.C., and Thompson, G.A., 1980, Mode and mechanisms of plateau uplifts, in Bally, A.W., Bender, P.L., McGetchin, T.R., and Walcott, R.I., eds., *Dynamics of Plate Interiors: American Geophysical Union Geodynamics Monograph 1*, p. 99–110, <https://doi.org/10.1029/GD001p0099>.
- McQuarrie, N., and Chase, C.G., 2000, Raising the Colorado Plateau: *Geology*, v. 28, no. 1, p. 91–94, [https://doi.org/10.1130/0091-7613\(2000\)028<0091:RTCP>2.0.CO;2](https://doi.org/10.1130/0091-7613(2000)028<0091:RTCP>2.0.CO;2).
- Mitrovica, J.X., Beaumont, C., and Jarvis, G.T., 1989, Tilting of continental interiors by the dynamical effects of subduction: *Tectonics*, v. 8, no. 5, p. 1079–1094, <https://doi.org/10.1029/TC008i005p01079>.
- Morgan, P., and Swanberg, C.A., 1985, On the Cenozoic uplift and tectonic stability of the Colorado Plateau: *Journal of Geodynamics*, v. 3, p. 39–63.
- Moucha, R., Forte, A.M., Rowley, D.B., Mitrovica, J.X., Simmons, N.A., and Grand, S.P., 2008, Mantle convection and the recent evolution of the Colorado Plateau and the Rio Grande Rift: *Geology*, v. 36, p. 439–442, <https://doi.org/10.1130/G24577A.1>.
- Nereson, A., Stroud, J., Karlstrom, K.E., and McIntosh, W.C., 2013, Dynamic topography of the western Great Plains: Geomorphic and $^{40}\text{Ar}/^{39}\text{Ar}$ evidence for mantle-driven uplift associated with the Jemez lineament of NE New Mexico and SE Colorado: *Geosphere*, v. 9, p. 521–545, <https://doi.org/10.1130/GES00837.1>.
- Nielson, J.E., Budahn, J.R., Unruh, D.M., and Wilshire, H.G., 1993, Actualistic models of mantle metasomatism documented in a composite xenolith from Dish Hill, California: *Geochimica et Cosmochimica Acta*, v. 57, p. 105–121, [https://doi.org/10.1016/0016-7037\(93\)90472-9](https://doi.org/10.1016/0016-7037(93)90472-9).
- Roy, M., Jordan, T.H., and Pederson, J., 2009, Colorado Plateau magmatism and uplift by warming of heterogeneous lithosphere: *Nature*, v. 459, p. 978–982, <https://doi.org/10.1038/nature08052>.
- Schutt, D.L., and Leshner, C.E., 2010, Compositional trends among Kaapvaal craton garnet peridotite xenoliths and their effects on seismic velocity and density: *Earth and Planetary Science Letters*, v. 300, no. 3–4, p. 367–373, <https://doi.org/10.1016/j.epsl.2010.10.018>.
- Schutt, D.L., Lowry, A.R., and Buehler, J.S., 2018, Moho temperatures and mobility of lower crust in the western United States: *Geology*, v. 46, p. 219–222, <https://doi.org/10.1130/G39507.1>.
- Shen, W., Ritzwoller, M.H., and Schulte-Pelkum, V., 2013, A 3-D model of the crust and uppermost mantle beneath the central and western US by joint inversion of receiver functions and surface wave dispersion: *Journal of Geophysical Research–Solid Earth*, v. 118, p. 262–276, <https://doi.org/10.1029/2012JB009602>.
- Sloss, L.L., 1963, Sequences in the cratonic interior of North America: *Geological Society of America Bulletin*, v. 74, no. 2, p. 93–114, [https://doi.org/10.1130/0016-7606\(1963\)74\[93:SITCIO\]2.0.CO;2](https://doi.org/10.1130/0016-7606(1963)74[93:SITCIO]2.0.CO;2).
- Smith, D., and Griffin, W.L., 2005, Garnetite xenoliths and mantle–water interactions below the Colorado Plateau: *Journal of Petrology*, v. 46, no. 9, p. 1901–1924, <https://doi.org/10.1093/ptrology/egi042>.
- Smyth, J.R., and Jacobsen, S.D., 2006, Nominally anhydrous minerals and Earth's deep water cycle, in Jacobsen, S.D., and van der Lee, S., eds., *Earth's Deep Water Cycle: American Geophysical Monograph 168*, <https://doi.org/10.1029/168GM02>.
- Spencer, J.E., 1996, Uplift of the Colorado Plateau due to lithosphere attenuation during Laramide low-angle subduction: *Journal of Geophysical Research–Solid Earth*, v. 101, p. 13,595–13,609, <https://doi.org/10.1029/96JB00818>.
- Tikoff, B., and Maxson, J., 2001, Lithospheric buckling of the Laramide foreland during Late Cretaceous and Paleogene, western United States: *Rocky Mountain Geology*, v. 36, no. 1, p. 13–35, <https://doi.org/10.2113/gsrocky.36.1.13>.
- Usui, T., Nakamura, E., Kobayashi, K., Maruyama, S., and Helmstaedt, H., 2003, Fate of the subducted Farallon plate inferred from eclogite xenoliths in the Colorado Plateau: *Geology*, v. 31, p. 589–592, [https://doi.org/10.1130/0091-7613\(2003\)031<0589:FOTSFP>2.0.CO;2](https://doi.org/10.1130/0091-7613(2003)031<0589:FOTSFP>2.0.CO;2).
- van der Lee, S., and Nolet, G., 1997, Upper mantle S velocity structure of North America: *Journal of Geophysical Research–Solid Earth*, v. 102, p. 22,815–22,838, <https://doi.org/10.1029/97JB01168>.
- Watts, A.B., 2012, Global Elastic Thickness Point Data and Grid: earth.ox.ac.uk/~tony/watts/downloads.htm (last accessed 22 November 2012).
- Whitmeyer, S.J., and Karlstrom, K.E., 2007, Tectonic model for the Proterozoic growth of North America: *Geosphere*, v. 3, p. 220–259, <https://doi.org/10.1130/GES00055.1>.
- Wong, I.G., and Humphrey, J.R., 1989, Contemporary seismicity, faulting, and the state of stress in the Colorado Plateau: *Geological Society of America Bulletin*, v. 101, p. 1127–1146, [https://doi.org/10.1130/0016-7606\(1989\)101<1127:CSFATS>2.3.CO;2](https://doi.org/10.1130/0016-7606(1989)101<1127:CSFATS>2.3.CO;2).
- Yuan, H., French, S., Cupillard, P., and Romanowicz, B., 2014, Lithospheric expression of geological units in central and eastern North America from full waveform tomography: *Earth and Planetary Science Letters*, v. 402, p. 176–186, <https://doi.org/10.1016/j.epsl.2013.11.057>.